molecular pharmaceutics

Article

pubs.acs.org/molecularpharmaceutics

# Cyclodextrin Complexes of Reduced Bromonoscapine in Guar Gum Microspheres Enhance Colonic Drug Delivery

Jitender Madan,[†] Sushma R. Gundala,[†] Bharat Baruah,[‡] Mulpuri Nagaraju,[§] Clayton Yates,[∥] Timothy Turner,[∥] Vijay Rangari,[⊥] Donald Hamelberg,[§] Michelle D. Reid,[#] and Ritu Aneja*[,†]

[†]Department of Biology and [§]Department of Chemistry, Georgia State University, Atlanta, Georgia 30303, United States
[‡]Department of Chemistry and Biochemistry, Kennesaw State University, Kennesaw, Georgia 30144, United States
[∥]Department of Biology and [⊥]Center for Advanced Materials, Tuskegee University, Tuskegee, Alabama 36088, United States
[#]Department of Pathology, Emory University School of Medicine, Atlanta, Georgia 30322, United States

Supporting Information

**ABSTRACT:** Here, we report improved solubility and enhanced colonic delivery of reduced bromonoscapine (Red-Br-Nos), a cyclic ether brominated analogue of noscapine, upon encapsulation of its cyclodextrin (CD) complexes in bioresponsive guar gum microspheres (GGM). Phase−solubility analysis suggested that Red-Br-Nos complexed with $\beta$-CD and methyl-$\beta$-CD in a 1:1 stoichiometry, with a stability constant ($K_c$) of $2.29 \times 10^3$ $M^{-1}$ and $4.27 \times 10^3$ $M^{-1}$. Fourier transforms infrared spectroscopy indicated entrance of an $O-CH_2$ or $OCH_3-C_6H_4-OCH_3$ moiety of Red-Br-Nos in the $\beta$-CD or methyl-$\beta$-CD cavity. Furthermore, the cage complex of Red-Br-Nos with $\beta$-CD and methyl-$\beta$-CD was validated by several spectral techniques. Rotating frame Overhauser enhancement spectroscopy revealed that the $H_a$ proton of the $OCH_3-C_6H_4-OCH_3$ moiety was closer to the $H_5$ proton of $\beta$-CD and the $H_3$ proton of the methyl-$\beta$-CD cavity. The solubility of Red-Br-Nos in phosphate buffer saline (PBS, pH ∼ 7.4) was improved by ∼10.7-fold and ∼21.2-fold when mixed with $\beta$-CD and methyl-$\beta$-CD, respectively. This increase in solubility led to a favorable decline in the $IC_{50}$ by ∼2-fold and ∼3-fold for Red-Br-Nos−$\beta$-CD-GGM and Red-Br-Nos−methyl-$\beta$-CD-GGM formulations respectively, compared to free Red-Br-Nos−$\beta$-CD and Red-Br-Nos−methyl-$\beta$-CD in human colon HT-29 cells. GGM-bearing drug complex formulations were found to be highly cytotoxic to the HT-29 cell line and further effective with simultaneous continuous release of Red-Br-Nos from microspheres. This is the first study to showing the preparation of drug-complex loaded GGMS for colon delivery of Red-Br-Nos that warrants preclinical assessment for the effective management of colon cancer.

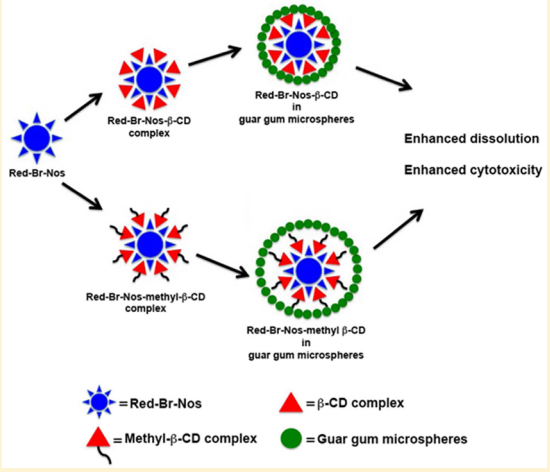


**KEYWORDS:** *Red-Br-Nos, colon cancer, β-cyclodextrin (β-CD), methyl-β-cyclodextrin (methyl-β-CD), guar gum microspheres (GGMs), cytotoxicity*

## INTRODUCTION

Noscapine suppresses the progression of human colon cancer cells by a mitochondrial mediated apoptosis pathway in a dose- and time-dependent manner.[1,2] Two newly synthesized brominated derivatives of noscapine, 9-Br-Nos (EM011) and Red-Br-Nos (EM012), have significant tubulin binding activity and influence tubulin polymerization in a different way from noscapine. The effect of 9-Br-Nos on inhibiting tubulin polymerization is superior to that of Red-Br-Nos. However, Red-Br-Nos captured cell cycle progression in the mitosis phase at lesser concentration (3.6 $\mu$M) than 9-Br-Nos (7.7 $\mu$M) and noscapine (18.4 $\mu$M) and consequently formed multipolar spindles. Hence, Red-Br-Nos, being a chemotherapeutic agent, has great potential to inhibit the progression of colon cancer cells.[3] Moreover, Red-Br-Nos is 5−40-fold more active than the parent compound, noscapine.[3,4] Although it has an excellent therapeutic profile, Red-Br-Nos, due to its lipophilic trait (log $P$ value ∼ 2.94), it is listed in the class II category of the armamentarium defined by the Biopharmaceutical Classification System (BCS).[5] Hence, the therapeutic benefits of Red-Br-Nos cannot be achieved in the physiological milieu of the colon and tumor compartment, until its solubility at the molecular level is improved. This necessitates the encapsulation of Red-Br-Nos in a bioresponsive, smart oral drug delivery system that can facilitate the release of drug in a solubilized form in colon (pH ∼ 5.5−7).[6]

Colon cancer tissue exhibits differential pathophysiology as compared to a healthy colon, where an acidic pH condition is

**Received:** June 9, 2014
**Revised:** October 24, 2014
**Accepted:** October 28, 2014
**Published:** October 28, 2014

  

observed in the former case due to the excessive secretion of bile fluid.[7] However, poor physicochemical and biopharmaceutical traits alter the diffusion of anticancer drugs in colon cancer tissue.[8] This may consequently enhance the dose size and side effects of chemotherapeutic drugs. Delivery of a high payload of chemotherapeutic drug selectively to the inner layer of colon may cause the tumor cells to subside and reduce the need of surgery.[9] This may be possible by customizing the oral controlled release bioresponsive drug delivery systems.

Owing to this unique property; an oral drug delivery system tailored with carbohydrate polymers would be ideal for colon targeting. This kind of drug delivery accommodates the possibility of self-administration and improved patient compliance while achieving and sustaining therapeutic doses of the drugs at the target site is considered effective. Currently, more than 60% of clinical drugs are administered via the oral route.[10]

Cyclodextrins (CDs) are widely used to study solubility and bioavailability issues and facilitate a biocompatible solid oral dosage form.[11] They are bucket-shaped, cyclic oligosaccharides composed of 6, 7, or 8 glucopyranose units, linked by $\alpha$, 1−4-glycosidic bonds.[12] $\beta$-CD, a unique molecule, has the ability to form stable soluble aggregates with a broad range of lipophilic molecules.[13,14] But the restricted aqueous solubility of $\beta$-CD (18.5 mg/mL) presents hurdles in the design and development of soluble complexes of lipophilic drugs.[15] As a substitute, methyl-$\beta$-cyclodextrin (methyl-$\beta$-CD) due to its wider cavity size and higher aqueous solubility (>2,000 mg/mL) produces more wettable amorphous complexes with improved water solubility.[16] Hence, we propose that cavitization of Red-Br-Nos using supramolecular chemistry would improve the dissolution of drug in physiological milieu of cancer cell compartments.

Several strategies have been applied to selectively steer the chemotherapeutic drugs to the colon via the oral route of administration including pH dependent drug delivery, prodrugs, and multiparticulate systems.[17−19] Guar gum microspheres (GGM) have also been investigated for their selective targeting and delivery properties.[20,21] Guar gum is a carbohydrate consisting of galactose and mannose, which can be easily degraded by *Bifidobacterium dentium* strain.[22]

Therefore, in the present investigation, we have tailored and optimized $\beta$-cyclodextrin ($\beta$-CD) and methyl-$\beta$-cyclodextrin (methyl-$\beta$-CD) soluble complexes of Red-Br-Nos following the freeze-drying technique.[23,24] The physical and chemical structure of the drug complex was characterized, followed by simulating the molecular dynamics to determine functionality of the aggregates and evaluate the relative binding affinities. Further, the optimized complexes were hybridized with guar gum microparticles and were tested for *in vitro* efficacy following dissolution testing and cell proliferation assays on HT-29, human colon cancer cells.

## EXPERIMENTAL SECTION

**Materials.** Red-Br-Nos, [(*R*)-9-bromo-5-((*S*)-4,5-dimethoxy-1,3-dihydroisobenzofuran-1-yl)-4-methoxy-6-methyl-5,6,7,8-tetrahydro-1,3-dioxolo-[4,5-*g*]-isoquinoline] was synthesized in our laboratory.[3,4] Beta-cyclodextrin ($\beta$-CD), methyl-$\beta$-CD, DCl (35 wt % in $D_2O$, 99 atom % D), 3-[4,5-dimethylthiazol-2-yl]-2,5-diphenyltetrazolium bromide (MTT), phosphate buffered saline (PBS), guar gum, Dulbecco's modified Eagle's medium (DMEM), and fetal bovine serum were procured from Sigma-Aldrich. $D_2O$ (D 99.9%) and dimethyl sulfoxide-$d_6$ (DMSO-$d_6$) (D, 99.9% + 1% v/v TMS) were obtained from Cambridge Isotope Laboratories, Inc. NaOD (40 wt % in $D_2O$, 99+ atom % D) was procured from Acros Organics. All other chemicals used were of the highest analytical grade and used without further purification as provided by the manufacturer.

**Reagents and Cell Lines.** Human colon cancer (HT-29) cells (ATCC) were maintained in 5% $CO_2$ and 95% air at 37 °C using DMEM enriched with 10% fetal bovine serum. The experiments were carried out as described earlier.[25]

**Synthesis and Characterization of Red-Br-Nos-CDs Complexes.** *Phase Solubility Analysis.* The chemical nature of drug with cyclodextrins in the binary state was accredited by phase−solubility assay.[26] 20 mg of Red-Br-Nos was dispersed in 10 mL of PBS consisting of $\beta$-CD and methyl-$\beta$-CD respectively at various concentrations (1−17 mM). In an orbital shaker (200 rpm, at 37 ± 1 °C) the samples were then stirred for equilibration for 5 days. Subsequently, the samples were filtered separately through 0.22 $\mu$m membrane filters (Millipore, Germany), and their absorbance at 291 nm was measured using a UV−visible spectrophotometer (Beckman Coulter). The slope of the phase−solubility diagram was used to calculate their apparent stability constant (eq 1):

$$K_c = \text{slope}/S_o(1 - \text{slope}) \quad (1)$$

where $K_c$ is the apparent stability constant and $S_o$ is the solubility of drug in cyclodextrin's absence.

*Preparation of Solid Complexes.* 1:1 ratios (mM) of Red-Br-Nos with (a) $\beta$-CD and (b) methyl-$\beta$-CD were separately mixed in the aqueous state at pH ∼ 4.5 to prepare solid complexes of Red-Br-Nos with CDs,[23,24] which were then mixed for 24 h on an orbital shaker at 200 rpm and 37 ± 1 °C, followed by freeze-drying. The mixtures then were passed through sieve #100 and collected as dry samples. Physical mixtures of Red-Br-Nos with $\beta$-CD and methyl-$\beta$-CD in 1:1 molar ratio were prepared by stirring and filtering through a #100 sieve to obtain the fine powder.

**Characterization of Solid Complexes.** *Fourier Transform Infrared (FT-IR) Spectroscopy.* FT-IR spectroscopy was used to characterize the solid complexes of Red-Br-Nos with $\beta$-CD and methyl-$\beta$-CD. Using an infrared spectrophotometer (PerkinElmer), the spectra of Red-Br-Nos, $\beta$-CD, methyl-$\beta$-CD, combinations of Red-Br-Nos with $\beta$-CD (1:1 mM) and methyl-$\beta$-CD (1:1 mM), and aggregates of Red-Br-Nos with $\beta$-CD (Red-Br-Nos−$\beta$-CD) and methyl-$\beta$-CD (Red-Br-Nos−methyl-$\beta$-CD) (1:1 mM) were obtained. Samples were prepared in a KBr disk (2 mg of sample/200 mg of KBr) with a hydrostatic press at a force of 40 psi for 4 min. A scanning range of 400−4000 $cm^{-1}$ with a resolution of 4 $cm^{-1}$ was used.

*Differential Scanning Calorimetry (DSC).* The formation of aggregates in the solid phase was confirmed using DSC analysis. A differential scanning calorimeter (Mettler-Toledo Thermal Equipment) was used to document the endothermic peaks of Red-Br-Nos, $\beta$-CD, methyl-$\beta$-CD, mixtures of Red-Br-Nos with $\beta$-CD (1:1) and methyl-$\beta$-CD (1:1), and aggregates of Red-Br-Nos with $\beta$-CD (Red-Br-Nos−$\beta$-CD) and methyl-$\beta$-CD (Red-Br-Nos−methyl-$\beta$-CD) (1:1 mM). Nitrogen gas was maintained at 50 mL/min (flow rate). Thermograms were traced using 10 mg of sample with heating rate of 19.99 °C/min in the 30 to 300 °C temperature range.

*Powder X-ray Diffraction Pattern (PXRD).* The organization of bonds in the crystal lattice of Red-Br-Nos, $\beta$-CD, methyl-$\beta$-CD, mixtures of Red-Br-Nos with $\beta$-CD (1:1 mM) and methyl-$\beta$-CD (1:1 mM), and aggregates of Red-Br-Nos with $\beta$-CD (Red-Br-Nos−$\beta$-CD) and methyl-$\beta$-CD (Red-Br-Nos−methyl-$\beta$-CD) was determined as described earlier.[23,24]

*Scanning Electron Microscopy (SEM).* The surface topography of Red-Br-Nos, $\beta$-CD, methyl-$\beta$-CD, mixtures of Red-Br-Nos with $\beta$-CD (1:1 mM) and methyl-$\beta$-CD (1:1 mM), and the Red-Br-Nos complexes with $\beta$-CD (Red-Br-Nos−$\beta$-CD) and methyl-$\beta$-CD (Red-Br-Nos−methyl-$\beta$-CD) was captured as described earlier.[23,24]

*Nuclear Magnetic Resonance ($^1$H NMR) Spectroscopy.* The changes in chemical shift before and after complexation in the solid state were observed using a BRUKER DPX 300 MHz spectrometer by recording $^1$H NMR spectra as described earlier.[23,24]

**Molecular Dynamics Simulations and *in Silico* Molecular Modeling.** The 3D (three-dimensional) crystal structure of $\beta$-CD was taken from PDBID 3M3R[27] (2.20 Å) to apply molecular dynamics simulations and docking techniques as described earlier.[23,24,28−36]

**Determination of Encapsulation Efficiency.** The encapsulation efficiency of Red-Br-Nos−$\beta$-CD and Red-Br-Nos−methyl-$\beta$-CD complexes was determined by dissolving separately 5 mg of sample in 100 mL of phosphate buffered saline as described earlier.[23,24] The absorbance of supernatant was then recorded at 291 nm on a UV−visible spectrophotometer (Beckman Coulter). The following formula was used to calculate percent efficiency of encapsulation:

$$\%\ \text{encapsulation efficiency} = \frac{\text{practical value}}{\text{theoretical value}} \times 100$$

**Evaluation of Aqueous Phase Solubility.** The solubility of drug and aggregates in the aqueous state was evaluated using saturated solutions as described previously.[23,24] Triplicates of experiments were performed ($n$ = 3).

**Preparation and Characterization of Red-Br-Nos-CD Complex Loaded Guar Gum Microspheres.** Red-Br-Nos, Red-Br-Nos−$\beta$-CD, and Red-Br-Nos−methyl-$\beta$-CD loaded guar gum microspheres designated as Red-Br-Nos-GGM, Red-Br-Nos−$\beta$-CD-GGM, and Red-Br-Nos−methyl-$\beta$-CD-GGM were prepared by an emulsion polymerization technique.[20,23,24]

**Particle Size Analysis.** A zetasizer, HAS 3000 (Malvern Instruments, Worcestershire, U.K.), was employed to subject the microspheres to particle size analysis. For measuring particle size, a 5 mg sample of the microspheres was dissolved in PBS (5 mL) followed by adjusting the pH up to 7.4. All measurements were made at 25 °C in triplicate ($n$ = 3).

**Scanning Electron Microscopy.** The scanning electron microscopy of all three formulations of guar gum microspheres was carried out following the conditions as specified earlier.[23,24]

**Determination of Encapsulation Efficiency.** 50 mg samples of all three guar gum microsphere formulations were dissolved separately in 0.02 N hydrochloric acid (50 mL each). Suspensions were mildly heated for 10−15 min and left to settle for 72 h. Subsequently, microspheres were centrifuged at 15000 rpm and filtered through a 0.22 $\mu$m membrane filter (Millipore, Germany), and a sample of the filtrate diluted using 0.02 N HCl was analyzed at 291 nm in a UV/visible spectrophotometer (Beckman Coulter) to evaluate the amount of Red-Br-Nos entrapped in microspheres. All experiments were conducted at 25 °C in triplicate ($n$ = 3).

***In Vitro* Testing of Optimized Complexes and Complex Loaded Guar Gum Microspheres Following Dissolution and Cell Proliferation Assay.** *Dissolution Testing.* Dissolution tests were conducted using a type II USP dissolution test apparatus. The dissolution study of Red-Br-Nos, physical mixtures of Red-Br-Nos with $\beta$-CD and methyl-$\beta$-CD, and respective complexes was conducted as specified earlier.[23,24,37]

The release studies of Red-Br-Nos-GGM, Red-Br-Nos−$\beta$-CD-GGM, and Red-Br-Nos−methyl-$\beta$-CD-GGM were performed in simulated intestinal fluids ($KH_2PO_4$ ∼ 68.04 g, NaOH ∼ 8.96 g, and deionized water ∼ 10 L, pH 6.8, without enzyme) and simulated colonic fluid (KCl ∼ 0.20 g/L, NaCl ∼ 8 g/L, $KPO_4$ monobasic ∼ 0.24 g/L, $Na_2PO_4$ dibasic ∼ 1.44 g/L, pH 7.0) comprising 2% and 6% w/v rat cecal matter, with and without enzyme induction to simulate *in vivo* colon environment as previously described.[23,24]

*In Vitro Cell Growth Inhibition Assay.* MTT (3-(4,5-dimethylthiazol-2-yl)-2,5-diphenyltetrazolium bromide) assay[38] was performed using HT-29 (human colon cancer cell line) to determine the proliferative capacity of cells treated with Red-Br-Nos, $\beta$-CD, methyl-$\beta$-CD, Red-Br-Nos−$\beta$-CD complex, Red-Br-Nos−methyl-$\beta$-CD complex, Red-Br-Nos-GGM, Red-Br-Nos−$\beta$-CD-GGM, and Red-Br-Nos−methyl-$\beta$-CD-GGM. The blank microspheres were used as control.[23,24]

*Statistical Analysis.* Student $t$-test and one-way analysis of variance were employed to analyze the statistical significance. $p < 0.05$ was considered to be a substantial difference. All the data is represented as average ± SD for $n \geq 3$.

## RESULTS

**Synthesis and Characterization of Red-Br-Nos Aggregates in Solution and Solid-State Determination of Their Stoichiometry.** The primary objective of the current study was to formulate a unique hybridized microparticulate drug delivery system that can improve the colonic bioavailability of Red-Br-Nos to impart therapeutic action. Therefore, we utilized the biocompatible glucose cyclic oligomers, CD, to encapsulate Red-Br-Nos using inclusion chemistry to enhance the dissolution and solubility phenomena. The drug delivery at the site of action was improved by hybridizing the optimized drug−CD complex with bioresponsive guar gum microspheres. In the present investigation, we have explored supramolecular coupling techniques to enhance the solubility of Red-Br-Nos in physiological milieu via the freeze-drying-based cycloencapsulation method.[23,24] First, we determined the stoichiometry along with apparent stability constant ($K_c$) of tailored aggregates. Therefore, phase−solubility analysis was employed to calculate the stoichiometry in the solution phase.[26] The phase−solubility curves of Red-Br-Nos in $\beta$-CD and methyl-$\beta$-CD complexes in solution phase are represented in Figure 1. The curves show a proportional hike in solubility of Red-Br-Nos with increasing concentrations of $\beta$-CD and methyl-$\beta$-CD, respectively. Hence, the solubility curves of Red-Br-Nos with $\beta$-CD and methyl-$\beta$-CD can be classified as $A_L$

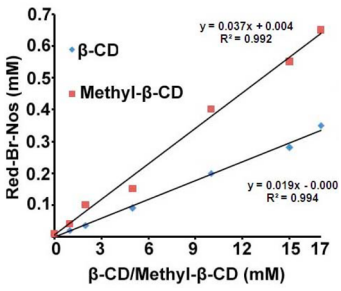


**Figure 1.** Phase−solubility analysis of binary system of Red-Br-Nos with $\beta$-CD and methyl-$\beta$-CD, respectively.


dx.doi.org/10.1021/mp500408n | *Mol. Pharmaceutics* 2014, 11, 4339−4349

type.[11] The linear curves of Red-Br-Nos with β-CD and methyl-β-CD suggested the formation of a 1:1 complex in the solution phase. The stability constants ($K_c$) of the binate systems of Red-Br-Nos with β-CD and methyl-β-CD were determined to be 2.29 × $10^3$ $M^{-1}$ and 4.27 × $10^3$ $M^{-1}$, respectively, from the phase−solubility linear plots (Figure 1).

**Conformation of Complexes in the Solid Phase.** Following phase−solubility analysis, the complexes of Red-Br-Nos with β-CD and methyl-β-CD were characterized in the solid state with FTIR spectroscopy. The hydrophobic association induced alterations in the stretching frequencies amid the cycloencapsulation of Red-Br-Nos in the β-CD and methyl-β-CD cavities were analyzed by recording the spectra. The stretching frequencies of Red-Br-Nos, β-CD, methyl-β-CD, mixtures, and the aggregates are shown in Table 1 and Suppl. Figure 1 in the Supporting Information. The FT-IR spectrum of Red-Br-Nos revealed a distinctive peak at 1,032 $cm^{-1}$, emphasizing the presence of ortho-substituted benzene. Peaks at 1,418 and 1,380 $cm^{-1}$ for N−$CH_3$ bending pulsations and 2,949, 2,853, and 2,701 $cm^{-1}$ because of the presence of various $OCH_3$/$CH_3$ groups were observed for Red-Br-Nos. The β-CD gamut presented the pulsation of free −OH groups at 3,281 $cm^{-1}$ whereas 2,925 and 1,640 $cm^{-1}$ signified the existence of −CH stretching and H−O−H bending. But, the peak at 2,835 $cm^{-1}$ in methyl-β-CD ($OCH_3$/$OCH_2$) distinguished it from β-CD. The mixture of Red-Br-Nos with β-CD and methyl-β-CD denoted that 2949 and 2853 $cm^{-1}$ ($OCH_3$/$CH_3$ groups) peaks of Red-Br-Nos were masked; however few identical peaks of individual components were also present. Further, the distinctive peaks (2949 and 2853 $cm^{-1}$) were masked by introduction of Red-Br-Nos in the β-CD and methyl-β-CD nanocavities by complex formation. This suggested the introduction of methoxy group in the cyclodextrin pocket. Hence, the infrared spectra initially indicated the involvement of functional groups of Red-Br-Nos that infiltrate the β-CD and methyl-β-CD pockets. To further corroborate the synthesis of Red-Br-Nos complexes with β-CD and methyl-β-CD in the solid phase, DSC was employed to determine the endothermic peaks in comparison to their individual components as shown in Figure 2. The endothermic peak of Red-Br-Nos was found at 168.83 °C, similar to noscapine's melting point (170−175 °C). The CD thermograms (i.e., α-, β-, and γ-CDs) indicate a wide peak range from 40 to 150 °C (117.83 °C for β-CD and 83 °C for methyl-β-CD) because of the evaporation of water molecules. The thermograms of Red-Br-Nos and β-CD mixture as well as methyl-β-CD mixture specified that identical peaks of individual components were present in the mixtures. However, the endothermic peaks of Red-Br-Nos became invisible in the thermograms of Red-Br-Nos−β-CD and Red-Br-Nos−methyl-β-CD aggregates with an alteration in the peaks of β-CD and methyl-β-CD to 72.5 °C and 100.83 °C.

**PXRD Characterization of Complexes.** Next, we identified the crystalline configurations of Red-Br-Nos in the nano-encapsulation mode by the PXRD technique. Similar to noscapine, the XRD pattern of Red-Br-Nos exhibited acute peaks signifying the crystalline pattern (Figure 3A−G). Though β-CD's pattern was associated with acute peaks representing its crystalline nature, the introduction of methylation in β-CD (methyl-β-CD) changed the crystalline configuration into an amorphous phase revealing broad and dispersed peaks, ascertaining the enhanced solubility of methyl-β-CD in the aqueous phase in comparison with β-CD. Red-Br-Nos and β-CD as well as methyl-β-CD physical mixture's XRD pattern confirmed that the peaks for individual components are present.

**Table 1. FTIR Spectrum Assignment of Red-Br-Nos, β-CD, Methyl-β-CD, Physical Mixtures, and Red-Br-Nos−β-CD and Red-Br-Nos−Methyl-β-CD Inclusion Complexes, Measured between 4400 and 400 $cm^{-1}$**

| peaks ($cm^{-1}$) | assignment | peaks ($cm^{-1}$) | assignment |
|---|---|---|---|
| Red-Br-Nos[a] | | inclusion complex (Red-Br-Nos−β-CD) | |
| 2949, 2853, 2701 | (ν, −$OCH_3$/$OCH_2$) | 2927 | (−CH stretching) |
| 1636 | | 1615 | |
| 1614 | | 1449 | |
| 1448 | | 1154 | (C−H stretching) |
| 1418, 1380 | (ν, N−$CH_3$) | 1082 | (C−O stretching) |
| 1265 | | 1037 | (C−O−C bending) |
| 1224 | | methyl-β-CD[c] | |
| 1076 | | 2925 | (−CH stretching) |
| 1032 | (ν, ortho substituted benzene) | 2835 | (ν, −$OCH_3$/$OCH_2$) |
| β-CD[b] | | 1638 | (H−O−H bending) |
| 3281 | (−OH stretching) | 1154 | (C−H stretching) |
| 2925 | (−CH stretching) | 1083 | (C−O stretching) |
| 1640 | (H−O−H bending) | 1033 | |
| 1152 | (C−H stretching) | physical mixture (Red-Br-Nos and methyl-β-CD) | |
| 1077 | (C−O stretching) | 2925 | (C−O−C bending) |
| 1022 | (C−O−C bending) | 1615 | (ν, −CH stretching) |
| physical mixture (Red-Br-Nos and β-CD) | | 1449 | |
| 3293 | (−OH stretching) | 1155 | (C−H stretching) |
| 2920 | (ν, −CH stretching) | 1079 | |
| 1637 | | 1034 | (C−O−C bending) |
| 1449 | | inclusion complex (Red-Br-Nos−methyl-β-CD) | |
| 1153 | (C−H stretching) | 2926 | (ν, −CH stretching) |
| 1077 | | 1616 | |
| 1026 | (C−O−C bending) | 1492 | |
| | | 1445 | |
| | | 1031 | (C−O−C bending) |

[a]Reduced bromonoscapine. [b]Beta-cyclodextrin. [c]Methyl-beta-cyclodextrin.

However, owing to overlapping effect, Red-Br-Nos maintained its initial crystallinity in physical mixture with methyl-β-CD. Lastly the complexes of Red-Br-Nos with β-CD and methyl-β-CD exhibited peaks of decreasing intensity. Major shifts that occurred in crystalline peaks of Red-Br-Nos upon encapsulation in physical mixtures and complexation with β-CD and methyl-β-CD are depicted in Suppl. Table 1 in the Supporting Information.

**SEM Characterization.** Surface texture of complexes was observed using SEM (Figure 4A−G). However, this technique is not a confirmation of the solid-state complex synthesis, but facilitates the examination of the occurrence of a single entity in the complex. This technique confirmed the presence of regular sized crystalline particles in Red-Br-Nos, an observation

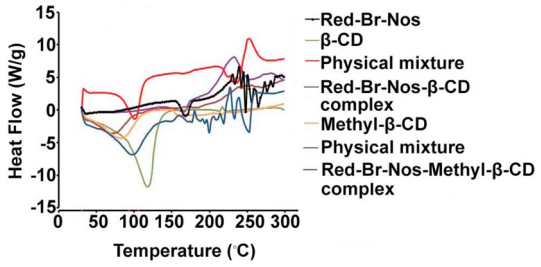


**Figure 2.** Differential scanning calorimetry analysis of Red-Br-Nos, $\beta$-CD, physical mixture, Red-Br-Nos−$\beta$-CD complex, methyl-$\beta$-CD, physical mixture, and Red-Br-Nos−methyl-$\beta$-CD complex.

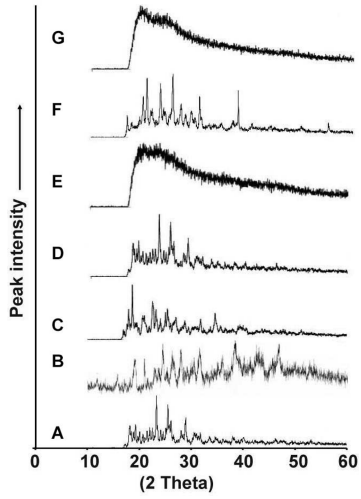


**Figure 3.** PXRD pattern of (A) Red-Br-Nos, (B) $\beta$-CD, (C) physical mixture of Red-Br-Nos and $\beta$-CD, (D) Red-Br-Nos−$\beta$-CD complex, (E) methyl-$\beta$-CD, (F) physical mixture of Red-Br-Nos and methyl-$\beta$-CD, and (G) Red-Br-Nos−methyl-$\beta$-CD complex.

consistent with the PXRD results. Also, crystalline particles of $\beta$-CD were found to have vague structures. The mixture of Red-Br-Nos with $\beta$-CD demonstrated adherence of the individual crystalline component, which indicated the efficient mixing. However, the complex of Red-Br-Nos with $\beta$-CD exhibited narrow sized particles with an aggregate forming tendency, proposing the presence of amorphous product. On the other hand, methyl-$\beta$-CD exists in an amorphous lattice instead of a crystalline structure, like native polymer. Hence, the physical mixture of Red-Br-Nos with methyl-$\beta$-CD illustrated the existence of both crystalline and amorphous particles, while the complex Red-Br-Nos−methyl-$\beta$-CD substantiated the presence of an amorphous product alone.

**NMR Spectroscopy for Characterization of Complexes.** Solution phase characterization of the complexes was conducted using $^1$H NMR spectroscopy. According to the chemical shift variations, $^1$H NMR communicates data on free and bound phases of a guest compound. The resultant chemical shift, $\Delta\delta$, is represented as variation between bound and free guest molecule chemical shifts. Such resultant shifts were measured by applying the formula $\Delta\delta = \delta_{complex} - \delta_{free}$.[39] The positive and negative signs based on this equation indicated downfield and upfield shifts, respectively. The $^1$H NMR spectra of free $\beta$-CD and methyl-$\beta$-CD with their designated aggregates in $D_2O$ are shown in Figure 5B,C. Since $H_3$ and $H_5$ protons located in the nanocavities of $\beta$-CD and methyl-$\beta$-CD, their signals were found to shift upfield due to interaction with guest molecule, Red-Br-Nos, revealing the formation of complex through the inclusion mode. Also, the shift in the signals for the protons $H_1$, $H_2$, $H_4$, and $H_6$ existing on the exterior of $\beta$-CD and methyl-$\beta$-CD indicated the host molecule's conformational change in the presence of guest compound, as shown in Table 2. Furthermore, through-space intermolecular interactions in the CD complexes were confirmed by $^1$H−$^1$H 2D ROESY experiments.[40] Red-Br-Nos interactions with $\beta$-CD and methyl-$\beta$-CD were also evaluated by $^1$H−$^1$H 2D ROESY and presented as partial contour graphs in Figure 5B,C. The correlation between the $H_a$ proton of Red-Br-Nos with the inner proton $H_5$ of $\beta$-CD and $H_3$ of methyl-$\beta$-CD has been represented. However, other protons of Red-Br-Nos and CDs exhibited no correlations, and this ascertained that a Red-Br-Nos ring was partially inserted, excluding other aromatic protons into the nanocavity. The spectrum indicated that Red-Br-Nos deeply penetrated the $\beta$-CD and methyl-$\beta$-CD nanocavities.

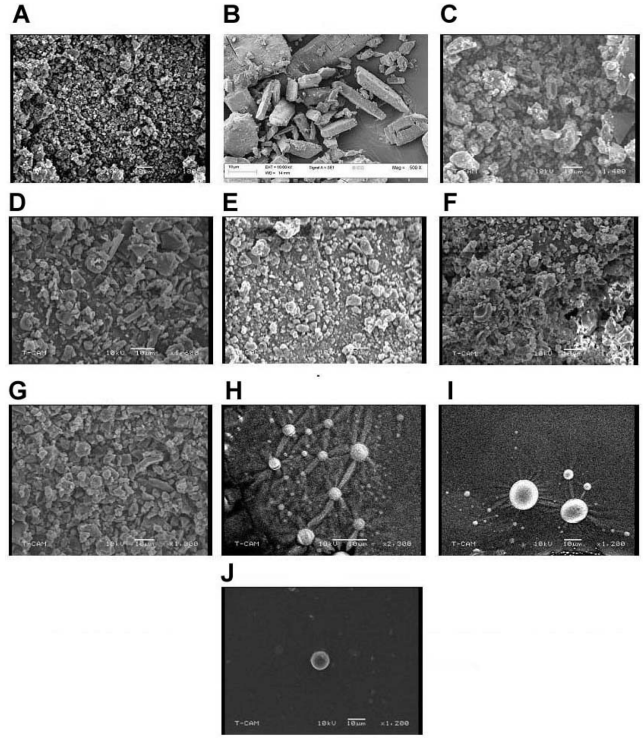


**Figure 4.** Scanning electron microscopy of (A) Red-Br-Nos, (B) $\beta$-CD, (C) physical mixture of Red-Br-Nos and $\beta$-CD, (D) Red-Br-Nos−$\beta$-CD complex, (E) methyl-$\beta$-CD, (F) physical mixture of Red-Br-Nos and methyl-$\beta$-CD, (G) Red-Br-Nos−methyl-$\beta$-CD complex, (H) Red-Br-Nos loaded guar gum microspheres, (I) Red-Br-Nos−$\beta$-CD complex loaded guar gum microspheres, and (J) Red-Br-Nos−methyl-$\beta$-CD complex loaded guar gum microspheres.

***In Silico* Docking and Molecular Dynamics Simulation for Characterization of Complexes.** We used *in silico* docking and molecular dynamics simulation to evaluate the complexation of Red-Br-Nos with $\beta$-CD and methyl-$\beta$-CD. This study suggested that the $H_3CO-C_6H_4-OCH_3$ group of Red-Br-Nos was in the $\beta$-CD nanocavity, while the Br-attached ring was resolved along the wider edge of $\beta$-CD in both the aggregates (Red-Br-Nos−$\beta$-CD and Red-Br-Nos−methyl-$\beta$-CD). These structures were used as starting conformations to determine the molecular dynamics simulations (Figure 6B). For each complex, at least 40,000 conformations were generated in MD simulations. The interaction binding free energy of every simulation was


dx.doi.org/10.1021/mp500408n | *Mol. Pharmaceutics* 2014, 11, 4339−4349

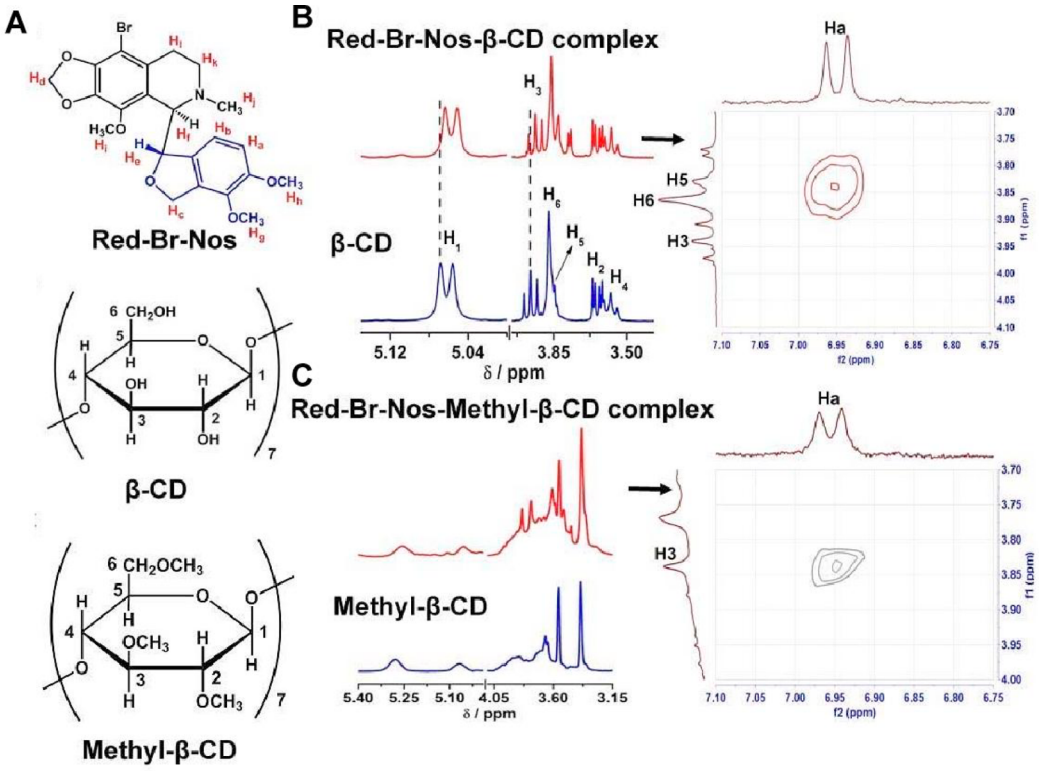


**Figure 5.** (A) Schematic representation of chemical structure of Red-Br-Nos, $\beta$-CD, and methyl-$\beta$-CD. (B) $^1$H 1D spectra of free $\beta$-CD and Red-Br-Nos−$\beta$-CD complex in $D_2O$ and partial contour plot of the $^1$H−$^1$H 2D ROESY spectrum of Red-Br-Nos−$\beta$-CD complex in $D_2O$. The correlation between proton $H_a$ of Red-Br-Nos and inner proton $H_5$ of $\beta$-CD has been shown. (C) $^1$H 1D spectra of free methyl-$\beta$-CD and Red-Br-Nos−methyl-$\beta$-CD complex in $D_2O$ and partial contour plot of the $^1$H−$^1$H 2D ROESY spectrum of Red-Br-Nos−methyl-$\beta$-CD complex in $D_2O$. The correlation between proton $H_a$ of Red-Br-Nos and inner proton $H_3$ of methyl-$\beta$-CD has been shown.

**Table 2. Chemical Shifts for the Protons of $\beta$-CD in the Free and Bound States**

| proton | $\beta$-CD (ppm)[a] | Red-9-Br-NOS−$\beta$-CD (ppm) | $\Delta\delta$ (ppm) |
|---|---|---|---|
| $H_1$ (d) | 5.0620 | 5.0599 | −0.0021 |
| $H_2$ (dd) | 3.6399 | 3.6418 | 0.0019 |
| $H_3$ (t) | 3.9604 | 3.9400 | −0.0204 |
| $H_4$ (t) | 3.5765 | 3.5758 | −0.0007 |
| $H_5$ (m) | 3.8450 | 3.8283 | −0.0167 |
| $H_6$ (d) | 3.8728 | 3.8638 | −0.0090 |

[a]Beta-cyclodextrin.

computed while dispersion of binding energies was also determined between Red-Br-Nos−$\beta$-CD and Red-Br-Nos−methyl-$\beta$-CD as shown in Figure 6A. The results suggested that Red-Br-Nos binds more efficiently to methyl-$\beta$-CD than $\beta$-CD as a similar trend was reported in the case of 9-Br-Nos, a tubulin binding anticancer agent and potential analogue of noscapine,[24] binding to CDs. However, the binding energies demonstrated that Red-Br-Nos is more favorable than 9-Br-Nos by 8−10 kcal/mol. The difference between 9-Br-Nos and Red-Br-Nos is that the C═O group of the five-membered lactone ring is replaced by a $-CH_2$ group (Figure 5A) that decreases the electrostatic potentials and increases the lipophilic trait of Red-Br-Nos. However, the electrostatic interaction contributions are almost the same in complex formation for 9-Br-Nos and Red-Br-Nos while the contribution of van der Waals interaction changes drastically (Figure 6A). The electrostatic and nonpolar input to the solvation free energy of Red-Br-Nos is about 2−4 kcal/mol and 1−2 kcal/mol more than that of 9-Br-Nos in both complexes (Figure 6A). The implications of these results reveal that the solvation destabilizes the Red-Br-Nos by 1−3 kcal/mol compared to 9-Br-Nos. However, Red-Br-Nos fabricates more stable complexes with $\beta$-CD and methyl-$\beta$-CD due to large variation in van der Waals interactions between Red-Br-Nos and 9-Br-Nos. The contribution of electrostatic and nonpolar solvation free energies are more in $\beta$-CD than that of methyl-$\beta$-CD, revealing the destabilization of Red-Br-Nos−$\beta$-CD/9-Br-Nos−$\beta$-CD compared to methyl-$\beta$-CD complexes. Consequently methyl-$\beta$-CD forms more stable complex with 9-Br-Nos and Red-Br-Nos than $\beta$-CD. The most plausible conformations of the Red-Br-Nos−$\beta$-CD and Red-Br-Nos−methyl-$\beta$-CD complexes are depicted in Figure 6B. The results reveal that Red-Br-Nos forms a firmer aggregate with methyl-$\beta$-CD than $\beta$-CD, with the $H_3CO-C_6H_4-OCH_3$ group of Red-Br-Nos in the CD nanocavity.

**Analysis of Solubility and Encapsulation Efficiency.** Upon characterization of the solid complexes, we next evaluated if the complexation rendered improved solubility of Red-Br-Nos. A substantial ($p < 0.05$) improvement in the solubility of the complexes of Red-Br-Nos with $\beta$-CD ($4.6 \times 10^{-3}$ g/mL) and methyl-$\beta$-CD ($9.1 \times 10^{-3}$ g/mL) was observed compared to free Red-Br-Nos, $0.43 \times 10^{-3}$g/mL. Quantitatively, the solubility of Red-Br-Nos upon complexation with $\beta$-CD and methyl-$\beta$-CD was enhanced by ∼10.7-fold and ∼21.2-fold, in comparison to free Red-Br-Nos. The encapsulation efficiency of Red-Br-Nos in $\beta$-CD and methyl-$\beta$-CD solid complexes was calculated to be 93.4% and 97.1%, respectively.

**Characterization of Complex Loaded Guar Gum Microspheres.** Red-Br-Nos and optimized complex loaded


dx.doi.org/10.1021/mp500408n | Mol. Pharmaceutics 2014, 11, 4339−4349

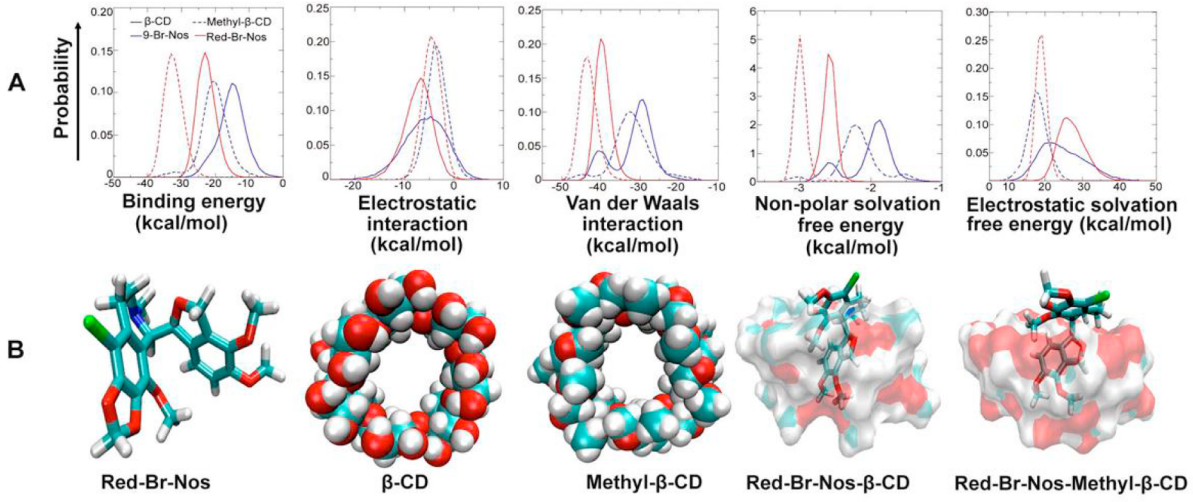


**Figure 6.** Complexation energies of Red-Br-Nos and 9-Br-Nos with $\beta$-CD and methyl-$\beta$-CD, measured as (A) binding energy (kcal/mol), electrostatic interaction energy (kcal/mol), van der Waals interaction energy (kcal/mol) of 9-Br-Nos and Red-Br-Nos with $\beta$-CD and methyl-$\beta$-CD, nonpolar solvation free energy and electrostatic solvation free energy (kcal/mol); and (B) conformation molecular modeling structures of Red-Br-Nos in $\beta$-CD and methyl-$\beta$-CD respectively.

guar gum microspheres were produced separately by the emulsion polymerization method[20] using chemical cross-linker glutaraldehyde to impart hardening to the microspheres. We used 2% w/v guar gum, 3% Span 80, 1.5 mL of glutaraldehyde, 50 °C temperature, 4000 rpm rotational speed, and 4 h stirring time for preparation of microspheres that ensured the optimal size of microspheres for oral drug delivery. The mean particle diameter of guar gum microspheres was observed to be 8.4 ± 2.02 $\mu$m, 12.5 ± 2.9 $\mu$m, and 16.5 ± 3.25 $\mu$m for Red-Br-Nos-GGM, Red-Br-Nos−$\beta$-CD-GGM, and Red-Br-Nos−methyl-$\beta$-CD-GGM formulations, respectively (Table 3). Stable dispersion of the polymer in oil phase was promoted using Span 80. Encapsulation efficiency was computed as ratio of amount of Red-Br-Nos in final microspheres (100 mg) to that of Red-Br-Nos introduced into the process. Percent encapsulation efficiency was calculated to be 65.84 ± 5.1% and 73.56 ± 4.3%, respectively for Red-Br-Nos−$\beta$-CD-GGM and Red-Br-Nos−methyl-$\beta$-CD-GGM, significantly ($p < 0.05$) higher than 40.36 ± 5.9% of Red-Br-Nos-GGM. Similarly, drug-loading capacity was calculated to be 5.04 ± 0.8 mg, 8.25 ± 0.9 mg, and 9.19 ± 0.5 mg per 10 mg of microspheres for Red-Br-Nos-GGM, Red-Br-Nos−$\beta$-CD-GGM, and Red-Br-Nos−methyl-$\beta$-CD-GGM formulations, respectively. Shape and surface morphology was determined by scanning electron microscopy (Figure 4H−J), which revealed that Red-Br-Nos-GGM consisted of a rough surface with spherical shape while Red-Br-Nos−$\beta$-CD-GGM and Red-Br-Nos−methyl-$\beta$-CD-GGM showed smooth surface, respectively.

**Table 3. Particle Size Analysis, Percent Encapsulation Efficiency, and Drug Loading Capacity of Red-Br-Nos-CDs Loaded Guar Gum Microspheres**

| | parameters | | |
|---|---|---|---|
| formulation | particle size[a] (mm) | % encapsulation effic[a] | drug loading capacity[a] (mg/10 mg) |
| Red-Br-Nos-GGM | 8.40 ± 2.02 | 40.36 ± 5.9 | 5.04 ± 0.8 |
| Red-Br-Nos−$\beta$-CD-GGM | 12.5 ± 2.90 | 65.84 ± 5.1 | 8.25 ± 0.9 |
| Red-Br-Nos−methyl-$\beta$-CD-GGM | 16.5 ± 3.25 | 73.56 ± 4.3 | 9.19 ± 0.5 |

[a]Each experiment was carried out in triplicate ($n = 3$).

**Analysis of Performance in Dissolution Testing and Cell Proliferation Assay.** *In Vitro Release Study.* Furthermore, dissolution studies of the tailored nanoformulations were carried out in PBS and artificial intestinal fluid (pH 6.8) as shown in Figure 7A−D. This data suggests that only 7.9% Red-Br-Nos was dispensed from the gelatin capsule filled with pure drug at 30 min as opposed to the Red-Br-Nos−$\beta$-CD and Red-Br-Nos−methyl-$\beta$-CD complex, which delivered significantly ($p < 0.05$) higher (70.9% and 90.6%) amounts of drug at similar intervals (Figure 7A). The physical mixtures of Red-Br-Nos with $\beta$-CD and methyl-$\beta$-CD however showed no significant affect ($p > 0.05$) on the drug release in comparison to pure drug. Subsequently, dissolution testing of complex loaded guar gum microspheres was conducted in artificial intestinal fluid (pH ∼ 6.8) (Figure 7B). The nanoformulations Red-Br-Nos−methyl-$\beta$-CD-GGM and Red-Br-Nos−$\beta$-CD-GGM released 30.4% and 24.8% of Red-Br-Nos, significantly ($p < 0.05$) higher than 14.5% by Red-Br-Nos-GGM, respectively.

Next simulated colonic fluid with 2% and 6% w/v cecal content was utilized to test the efficacy of the hybridized microspheres, in the presence and absence of enzyme induction. Furthermore, we observed 28.9% and 38.4% release of Red-Br-Nos from Red-Br-Nos−$\beta$-CD-GGM and 55.6% and 65.7% from Red-Br-Nos−methyl-$\beta$-CD-GGM respectively in 2% and 6% w/v rat cecal matter with no enzyme induction (Figure 7C). However, to further enhance the drug release from our formulations, we used artificial colonic fluid containing 2% and 6% w/v rat cecal matter with enzyme induction and obtained significantly improved results. Our formulation Red-Br-Nos−$\beta$-CD-GGM released 37.2% and 50.4% of Red-Br-Nos at 2% w/v and 6% w/v cecal matter while Red-Br-Nos−methyl-$\beta$-CD-GGM released 74.2% and 88.2% at 2% w/v and 6% w/v cecal matter concentration (Figure 7D).

*In Vitro Cytotoxicity Assay.* The cellular toxicity exerted by the formulations in human colon cancer cells, HT-29, was determined by MTT (3-[4,5-dimethylthiazol-2-yl]-2,5-diphenyl-tetrazolium bromide) cell viability assay by suspending the


dx.doi.org/10.1021/mp500408n | *Mol. Pharmaceutics* 2014, 11, 4339−4349

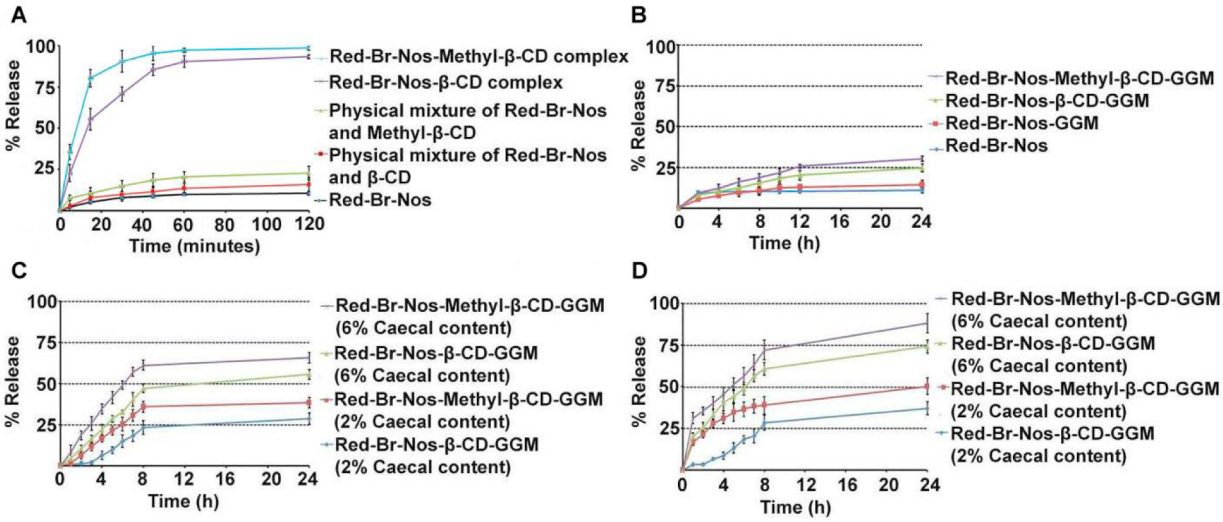


**Figure 7.** *In vitro* dissolution profile of (A) Red-Br-Nos, physical mixture of Red-Br-Nos and *β*-CD, Red-Br-Nos−*β*-CD complex, physical mixture of Red-Br-Nos and methyl-*β*-CD, and Red-Br-Nos−methyl-*β*-CD complex in phosphate buffered saline, pH 7.4. (B) Red-Br-Nos, Red-Br-Nos loaded guar gum microspheres, Red-Br-Nos−*β*-CD complex loaded guar gum microspheres, and Red-Br-Nos−methyl-*β*-CD complex loaded guar gum microspheres in simulated intestinal fluid, pH 6.8. (C) Red-Br-Nos−*β*-CD and methyl-*β*-CD complex loaded guar gum microspheres in 2% and 6% cecal content without enzyme induction in simulated colonic fluid, pH 7.0. (D) Red-Br-Nos−*β*-CD and methyl-*β*-CD complex loaded guar gum microspheres in 2% and 6% cecal content after enzyme induction in simulated colonic fluid, pH 7.0.

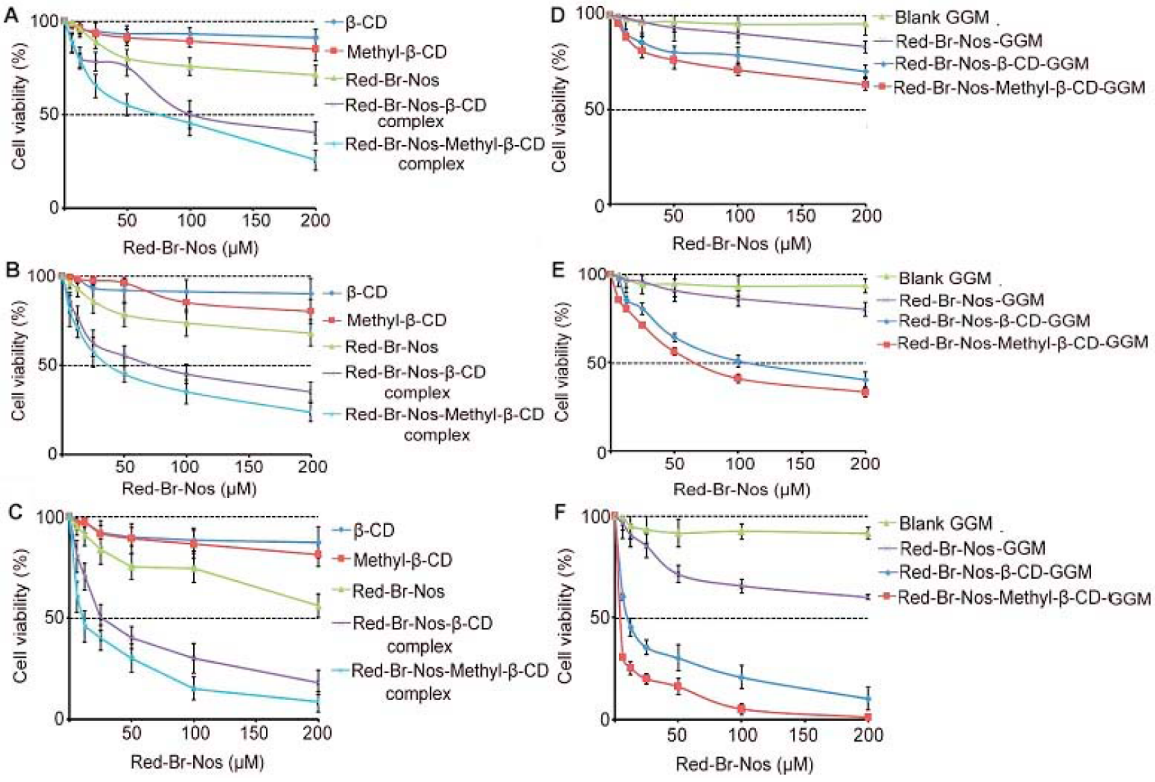


**Figure 8.** (A) Percent cell viability of Red-Br-Nos, *β*-CD, Red-Br-Nos−*β*-CD complex, methyl-*β*-CD, and Red-Br-Nos−methyl-*β*-CD complex at 24 h. (B) Red-Br-Nos, *β*-CD, Red-Br-Nos−*β*-CD complex, methyl-*β*-CD, and Red-Br-Nos−methyl-*β*-CD complex at 48 h. (C) Red-Br-Nos, *β*-CD, Red-Br-Nos−*β*-CD complex, methyl-*β*-CD, and Red-Br-Nos−methyl-*β*-CD complex at 72 h. (D) Blank guar gum microspheres, Red-Br-Nos−*β*-CD, and methyl-*β*-CD complex loaded guar gum microspheres at 24 h. (E) Blank guar gum microspheres, Red-Br-Nos−*β*-CD, and methyl-*β*-CD complex loaded guar gum microspheres at 48 h. (F) Blank guar gum microspheres, Red-Br-Nos−*β*-CD, and methyl-*β*-CD complex loaded guar gum microspheres at 72 h. Cytotoxicity study was carried out in phosphate buffer saline, pH 7.4.

formulations in PBS.[38] The $IC_{50}$ (11.9 $\mu$M) of Red-Br-Nos−methyl-*β*-CD was lower significantly compared to Red-Br-Nos−*β*-CD (27.1 $\mu$M) and Red-Br-Nos (~200 $\mu$M) at 72 h treatment. Next we observed the $IC_{50}$ of Red-Br-Nos and complex bearing guar gum microspheres for 24, 48, and 72 h. Compared to 72 h treatment with the free complexes, the complex bearing guar gum microspheres (Red-Br-Nos−methyl-*β*-CD-GGM, ~4.53 $\mu$M; Red-Br-Nos−*β*-CD-GGM, ~11.8 $\mu$M)


dx.doi.org/10.1021/mp500408n | *Mol. Pharmaceutics* 2014, 11, 4339−4349

exhibited significantly ($p < 0.05$) lower $IC_{50}$ than free complexes (Red-Br-Nos−methyl-$\beta$-CD, ~11.9 $\mu$M; Red-Br-Nos−$\beta$-CD, ~27.1 $\mu$M) (Figure 8D−F and Suppl. Figure 2 in the Supporting Information).

## DISCUSSION

Noscapine and its brominated derivatives (9-Br-Nos and Red-Br-Nos) have been investigated for anticancer potential against human colon cancer cells.[1−4] Reduction of the lactone ring in Red-Br-Nos remarkably improved the anticancer potential as compared to 9-Br-Nos and noscapine, however, it enhanced the lipophilicity of the drug. Hence, in the current study, Red-Br-Nos, a novel analogue of brominated noscapine, was cyclo-encapsulated in supramolecules like $\beta$-CD and methyl-$\beta$-CD to augment solubility and drug delivery for the management of colon cancer. The optimized complexes were then hybridized with guar gum microspheres to facilitate enhanced solubility and bioavailability at the site of action. Generally low molecular weight drugs are present at a ratio of 1:1 in CD molecule, with an individual molecule encapsulated within the nanocavity of a single CD molecule, associated with a dissociation constant of $K_{1:1}$ to attain equilibrium with respect to free and associated species.[11] Hence, the phase−solubility curve indicated that Red-Br-Nos established a 1:1 complex with $\beta$-CD and methyl-$\beta$-CD in binary aqueous phase (Figure 1). The phase−solubility curve can be categorized as $A_L$ kind revealing the resultant water-soluble aggregate with first-order kinetics for the formation of complex between Red-Br-Nos and CDs. Also, a variety of spectroscopic techniques were used to determine the structural configurations of complexes in the solid state. FT-IR spectral data exhibited that Red-Br-Nos was stable in the solid complex as there is no sign of any chemical linkage or degradation. Additionally, the FTIR spectra indicated that the inclusion mode may be presented as $-OCH_3$ or $-OCH_2$ group in CD nanocavities (Table 1). DSC thermograms ascertained the production of a 1:1 aggregate in the solid phase as an endothermic peak of Red-Br-Nos dissolved in the aggregates of $\beta$-CD and methyl-$\beta$-CD, in comparison to the peak of $\beta$-CD and methyl-$\beta$-CD (Figure 2). Also, PXRD patterns of Red-Br-Nos−$\beta$-CD and Red-Br-Nos−methyl-$\beta$-CD revealed peaks of moderate strength compared to spiky peaks of Red-Br-Nos (Figure 3). Correspondingly, noscapine[23] and brominated derivative of noscapine, 9-Br-Nos,[24] also exhibited characteristic sharp peaks from 20° to 40°. Next, PXRD pattern of $\beta$-CD and methyl-$\beta$-CD exhibited crystalline and amorphous geometry, consistent with the reported literature.[23,24] Hence, PXRD spectroscopy determined that Red-Br-Nos lies in the $\beta$-CD and methyl-$\beta$-CD pits as an amorphous polymer. Generally, due to erratic structural geometry, the amorphous phase involves minimal energy and thus renders maximum bioavailability to drugs.[41] Additionally, the SEM photomicrographs further verify the presence of Red-Br-Nos in an amorphous phase in $\beta$-CD and methyl-$\beta$-CD solid aggregates (Figure 4A−G). The solid complexes were further substantiated using 1D and 2D $^1$H NMR along with *in silico* docking studies followed by molecular dynamics simulations to evaluate the Red-Br-Nos complex conformations. $^1$H NMR spectroscopy provides evidence of aggregation between host and guest molecules in the solution state based on differences in chemical shift. Typically, when a guest molecule enters the host nanocavity, a considerable variation of the chemical environments is known to exist between free and bound phases. The chemical shift ($\delta$, ppm value) of a proton leans on the shielding constant while alterations in $\delta$ of the host and guest proton present a scale of complex formation extent. Since the chemical environment of few protons varies upon complexation, there is a subsequent difference in the chemical shifts ($\delta$ ppm) of $^1$H NMR resonance (shielding or deshielding effects). Thus, the chemical structure of complexes (Red-Br-Nos−$\beta$-CD and Red-Br-Nos−methyl-$\beta$-CD) was explicated with $^1$HNMR and ROESY spectroscopy. ROESY data deduced that the $H_a$ proton of $OCH_3-C_6H_4-CH_3O$ infiltrated the $\beta$-CD and methyl-$\beta$-CD nanocavities and thus can be correlated with the $H_5$ and $H_3$ protons of the nanocavities respectively (Figure 5). These data corresponded with the *in silico* molecular modeling (Figure 6). Also, the deshielding effect on Red-Br-Nos aromatic protons upon aggregate formation inferred that the drug permeated the host nanocavities (Table 2). A superior augmentation in Red-Br-Nos solubility by ~10.7-fold and ~21.2-fold during aggregation with $\beta$-CD and methyl-$\beta$-CD was noticed. Additionally, the aggregates displayed a favorable entrapment efficiency of Red-Br-Nos in $\beta$-CD and methyl-$\beta$-CD oriented complexes. Dissolution study was carried out in PBS and compared with free drug to justify the improved dissolution profile. Usually, alkaloid drugs (noscapinoids, $pK_a \sim 7.8$)[42] ionize at acidic pH of stomach and remain stringent at a neutral/basic/colon pH. We propose that Red-Br-Nos would have been undissociated at pH ~ 7.4 and inclusion into $\beta$-CD and methyl-$\beta$-CD nanocavities increased its solubility in dissolution medium. Thus, our data assured increased drug dissolution during aggregation with $\beta$-CD and methyl-$\beta$-CD, where an increased amount of drug was released in comparison to the free drug and physical mixtures (Figure 7A). This indicated the instant solubilization of Red-Br-Nos in intestinal/colon fluid. Next we analyzed the performance of dissolution of complex bearing guar gum microspheres in artificial intestinal (pH ~ 6.8) and colon (pH ~ 7.0) fluids containing 2% and 6% w/v cecal matter respectively with and without enzyme induction. The release profile of guar gum microspheres suggested that glutaraldehyde cross-linking decelerated the release of Red-Br-Nos from microspheres (Figure 7B). Glutaraldehyde reacts with hydroxyl group of galactose and mannose units of guar gum and, hence, resists water uptake by guar gum microspheres. Moreover, cross-linking decreases polymer chain mobility, improves glass transition temperature, and reduces diffusion.[20,21] An optimal drug delivery system targeting the colon must release the therapeutic amount of drug only in colon in post oral administration. A routine dissolution testing methodology cannot precisely predict *in vivo* efficacy of a colon-targeted drug delivery system. Hence, *in vitro* drug release studies were conducted in a modified artificial colon fluid release medium containing rat cecal content of about 2% w/v and 6% w/v concentrations, respectively, as reported in previous literature for guar gum microspheres, prepared with 2% w/v guar gum gel.[20] The quantity of fecal content of human colon is generally more than the concentration employed in the present study. The percent drug release was observed to be superior in the presence of rat cecal contents (with enzyme induction) as compared to other groups (Figure 7C,D). This may be attributed to greater degree of degradation of guar gum coating by colonic enzymes, present in cecal content that allowed higher drug release. Though the existence of rat cecal contents in simulated colon fluid (pH ~ 7.0) improved the Red-Br-Nos release, nevertheless, complete release of Red-Br-Nos was not achieved even after 24 h from Red-Br-Nos−$\beta$-CD-GGM and Red-Br-Nos−methyl-$\beta$-CD-GGM. Reduction in the enzymatic activity of polysaccharidases over longer duration of time may be accredited to the incomplete

release of Red-Br-Nos during *in vitro* testing.[43] The complexes of Red-Br-Nos with $\beta$-CD and methyl-$\beta$-CD and complex loaded guar gum formulations prevented the growth of HT-29 cells at lower $IC_{50s}$ in comparison to free drug, in congruence with the dissolution data. These drug complexes are likely to improve the drug diffusion across the plasma membrane as Red-Br-Nos is present in soluble un-ionized state in PBS (Figure 8A−C). Similarly, we also observed ∼2-fold and ∼3-fold lower $IC_{50}$ for Red-Br-Nos−$\beta$-CD-GGM and Red-Br-Nos−methyl-$\beta$-CD-GGM formulations in comparison to free Red-Br-Nos−$\beta$-CD and Red-Br-Nos−methyl-$\beta$-CD treated HT-29 cells (Figure 8D−F and Suppl. Figure 2 in the Supporting Information). Certainly, complex bearing guar gum microsphere formulations effectively inhibited the proliferation of HT-29 cells and this effect increased as Red-Br-Nos continued to be released from microspheres. The results suggest that the hybridized drug delivery system sufficiently perturbs the cellular membrane for diffusion to cause a cytostatic activity. It is proposed that this kind of drug delivery allows multiple and repetitious sites for drug−cell interactions.[44]

The current study outlines the chemistry of supramolecules (like $\beta$-CD and methyl-$\beta$-CD) to improve the cytotoxicity and solubility of Red-Br-Nos, a nontoxic, microtubule-modulating drug. Employing a wide variety of spectral and characterization techniques supported by computational analytics, our data confirms that the CD-based aggregates enhance the biological and physicochemical properties of Red-Br-Nos. Spherical, free-flowing glutaraldehyde cross-linked guar gum microspheres of complexes facilitated slow release of Red-Br-Nos in the colon, where the bacterial enzymes could degrade the guar gum from the microspheres, thus allowing the drug release at the target site. Hence, guar gum microsphere release of drug is a potential system for colon delivery of Red-Br-Nos, which warrants a detailed *in vivo* study in the future to design a novel therapeutic regimen for the management of colon cancer.

## ■ ASSOCIATED CONTENT

### Supporting Information

Suppl. Figure 1: FTIR spectrum of (A) Red-Br-Nos, (B) $\beta$-CD, (C) methyl-$\beta$-CD, (D) physical mixture of Red-Br-Nos and $\beta$-CD, (E) physical mixture of Red-Br-Nos and methyl-$\beta$-CD, (F) Red-Br-Nos−$\beta$-CD complex, and (G) Red-Br-Nos−methyl-$\beta$-CD complex. Suppl. Figure 2: Photomicrographs of (A) Red-Br-Nos suspension, (B) blank guar gum microsphere, (C) Red-Br-Nos loaded guar gum microsphere, (D) Red-Br-Nos−$\beta$-CD complex loaded guar gum microsphere, and (E) Red-Br-Nos−methyl-$\beta$-CD complex loaded guar gum microsphere treated HT-29 (human colon cancer cell line) cells at 24, 48, and 72 h. This material is available free of charge via the Internet at http://pubs.acs.org.

## ■ AUTHOR INFORMATION

### Corresponding Author

*Tel: 404-413-5417. Fax: 404-413-5300. E-mail: raneja@gsu.edu.

### Notes

The authors declare no competing financial interest.

## ■ ACKNOWLEDGMENTS

Grants to R.A. (J.M.) from the National Cancer Institute at the National Institutes of Health (1R00CA131489) supported this work in part. Grants to D.H. from NSF CAREER MCB-0953061 and the Georgia Cancer Coalition also supported this work in part.

## ■ REFERENCES

(1) Aneja, R.; Ghaleb, A. M.; Zhou, J.; Yang, V. W.; Joshi, H. C. p53 and p21 determine the sensitivity of noscapine-induced apoptosis in colon cancer cells. *Cancer Res.* **2007**, *67*, 3862−3870.

(2) Yang, Z. R.; Liu, M.; Peng, X. L.; Lei, X. F.; Zhang, J. X.; Dong, W. G. Noscapine induces mitochondria-mediated apoptosis in human colon cancer cells *in vivo* and *in vitro*. *Biochem. Biophys. Res. Commun.* **2012**, *421*, 627−633.

(3) Zhou, J.; Gupta, K.; Aggarwal, S.; Aneja, R.; Chandra, R.; Panda, D.; Joshi, H. C. Brominated derivatives of noscapine are potent microtubule-interfering agents that perturb mitosis and inhibit cell proliferation. *Mol. Pharmacol.* **2003**, *63*, 799−807.

(4) Zhou, J.; Liu, M.; Luthra, R.; Jones, J.; Aneja, R.; Chandra, R.; Tekmal, R. R.; Joshi, H. C. EM012, a microtubule-interfering agent, inhibits the progression of multidrug-resistant human ovarian cancer both in cultured cells and in athymic nude mice. *Cancer Chemother. Pharmacol.* **2005**, *55*, 461−465.

(5) Amidon, G. L.; Lennernas, H.; Shah, V. P.; Crison, J. R. A theoretical basis for a biopharmaceutics drug classification: the correlation of in vitro drug product dissolution and in vivo bioavailability. *Pharm. Res.* **1995**, *12*, 413−420.

(6) Chourasia, M. K.; Jain, S. K. Pharmaceutical approaches to colon targeted drug delivery systems. *J. Pharm. Pharm. Sci.* **2003**, *6*, 33−66.

(7) Thornton, J. R. High colonic pH promotes colorectal cancer. *Lancet* **1981**, *1*, 1081−1083.

(8) Lamprecht, A.; Yamamoto, H.; Takeuchi, H.; Kawashim, Y. Microsphere design for the colonic delivery of 5-fluorouracil. *J. Controlled Release* **2003**, *90*, 313−322.

(9) Jain, A.; Jain, S. K.; Ganesh, N.; Barve, J.; Beg, A. M. Design and development of ligand appended polysaccharidic nanoparticles for the delivery of oxaliplatin in colorectal cancer. *Nanomedicine* **2010**, *6*, 179−190.

(10) Nehal Siddiqui, M. D.; Garg, G.; Sharma, P. K. A short review on novel approaches in oral fast dissolving drug delivery system and their patents. *Adv. Biol. Res.* **2011**, *5*, 291−303.

(11) Stella, V. J.; Rajewski, R. A. Cyclodextrins: Their future in drug formulation and delivery. *Pharm. Res.* **1997**, *14*, 556−567.

(12) Hoda, A.; Sana, A. M.; Ola, A. K.; Ahmed, H. H. Characterization of ternary complexes of meloxicam-HP-$\beta$-CD and PVP or L-arginine prepared by the spray-drying technique. *Acta Pharm.* **2008**, *58*, 455−466.

(13) Soares da Silva, L. F.; do Carmo, F. A.; de Almeida Borges, V. R.; Monteiro, L. M.; Rodrigues, C. R.; Cabral, L. M.; de Sousa, V. P. Preparation and evaluation of lidocaine hydrochloride in cyclodextrin inclusion complexes for development of stable gel in association with chlorhexidine gluconate for urogenital use. *Int. J. Nanomed.* **2011**, *6*, 1143−1154.

(14) Celik, S. E.; Ozyurek, M.; Tufan, A. N.; Guclu, K.; Apak, R. Spectroscopic study and antioxidant properties of the inclusion complexes of rosmarinic acid with natural and derivative cyclodextrins. *Spectrochim Acta, Part A* **2011**, *78*, 1615−1624.

(15) Chatjigakis, A. K.; Donze, C.; Coleman, A. W.; Cardot, P. Solubility behavior of beta-cyclodextrin in water/cosolvent mixtures. *Anal. Chem.* **1992**, *64*, 1632−1634.

(16) Banchero, M.; Ronchetti, S.; Manna, L. Characterization of ketoprofen/methyl-$\beta$-cyclodextrin complexes prepared using supercritical carbon dioxide. *J. Chem.* **2013**, No. 583952.

(17) Esseku, F.; Adeyeye, M. C. Bacteria and pH-sensitive polysaccharide-polymer films for colon targeted delivery. *Crit. Rev. Ther. Drug Carrier Syst.* **2011**, *28*, 395−445.

(18) Krishnaiah, Y. S.; Khan, M. A. Strategies of targeting oral drug delivery systems to the colon and their potential use for the treatment of colorectal cancer. *Pharm. Dev. Technol.* **2012**, *17*, 521−540.

(19) Vaidya, A.; Jain, A.; Khare, P.; Agrawal, R. K.; Jain, S. K. Metronidazole loaded pectin microspheres for colon targeting. *J. Pharm. Sci.* **2009**, *98*, 4229−4236.

(20) Chaurasia, M.; Chourasia, M. K.; Jain, N. K.; Jain, A.; Soni, V.; Gupta, Y.; Jain, S. K. Cross-linked guar gum microspheres: a viable approach for improved delivery of anticancer drugs for the treatment of colorectal cancer. *AAPS PharmSciTech* **2006**, *7* (3), E143−E151 DOI: 10.1208/pt070374.
(21) Krishnaiah, Y. S. R.; Satyanarayana, V.; Dinesh Kumar, B.; Karthikeyan, R. S. *In vitro* drug release studies on guar gum-based colon targeted oral drug delivery systems of 5-fluorouracil. *Eur. J. Pharm. Sci.* **2002**, *16*, 185−192.
(22) Crociani, F.; Alessandrini, A.; Mucci, M. M.; Biavati, B. Degradation of complex carbohydrates by Bifidobacterium spp. *Int. J. Food Microbiol.* **1994**, *24*, 199−210.
(23) Madan, J.; Dhiman, N.; Parmar, V. K.; Sardana, S.; Bharatam, P. V.; Aneja, R.; Chandra, R.; Katyal, A. Inclusion complexes of noscapine in beta-cyclodextrin offer better solubility and improved pharmacokinetics. *Cancer Chemother. Pharmacol.* **2010**, *65*, 537−548.
(24) Madan, J.; Baruah, B.; Nagaraju, M.; Abdalla, M. O.; Yates, C.; Turner, T.; Rangari, V.; Hamelberg, D.; Aneja, R. Molecular cycloencapsulation augments solubility and improves therapeutic index of brominated noscapine in prostate cancer cells. *Mol. Pharmaceutics* **2012**, *9*, 1470−1480.
(25) Niv, Y.; Schwartz, B.; Amsalem, Y.; Lamprecht, S. A. Human HT-29 colon carcinoma cells: mucin production and tumorigenicity in relation to growth phases. *Anticancer Res.* **1995**, *15*, 2023−2027.
(26) de Melo, N. F.; Grillo, R.; Rosa, A. H.; Fraceto, L. F. Interaction between nitroheterocyclic compounds with beta-cyclodextrins: phase solubility and HPLC studies. *J. Pharm. Biomed. Anal.* **2008**, *47*, 865−869.
(27) Banerjee, A.; Mikhailova, E.; Cheley, S.; Gu, L. Q.; Montoya, M.; Nagaoka, Y.; Gouaux, E.; Bayley, H. Molecular bases of cyclodextrin adapter interactions with engineered protein nanopores. *Proc. Natl. Acad. Sci. U.S.A.* **2010**, *107*, 8165−8170.
(28) Dennington, R., II; Keith, T., Millam, J. *Gaussview, Version 3.09*; Semichem, Inc.: Shawnee Mission, KS, 2003.
(29) Trott, O.; Olson, A. J. AutoDock Vina: improving the speed and accuracy of docking with a new scoring function, efficient optimization, and multithreading. *J. Comput. Chem.* **2010**, *30*, 455−461.
(30) Case, D. A.; Darden, T. A., Cheatham, T. E.; Simmerling, C. L.; Wang, J.; Duke, R. E.; Luo, R.; Crowley, M.; Walker, R. C.; Zhang, W.; Merz, K. M.; Wang, B.; Hayik, S.; Roitberg, A.; Seabra, G.; Kolossváry, I.; Wong, K. F.; Paesani, F.; Vanicek, J.; Wu, X.; Brozell, S. R.; Steinbrecher, T.; Gohlke, H.; Yang, L.; Tan, C.; Mongan, J.; Hornak, V.; Cui, G.; Mathews, D. H.; Seetin, M. G.; Sagui, C.; Babin, V.; Kollman, P. A. *AMBER 10*; University of California: San Francisco, 2008.
(31) Jorgensen, W. L.; Chandrasekhar, J.; Madura, J. D.; Impey, R. W.; Klein, M. L. Comparison of simple potential functions for simulating liquid water. *J. Chem. Phys.* **1983**, *79*, 926−935.
(32) Kirschner, K. N.; Yongye, A. B.; Tschampel, S. M.; Daniels, C. R.; Foley, B. L.; Woods, R. J. GLYCAM06: a generalizable biomolecular force field. Carbohydrates. *J. Comput. Chem.* **2008**, *29*, 622−655.
(33) Wang, J.; Wolf, R. M.; Caldwell, J. W.; Kollman, P. A.; Case, D. A. Development and testing of a general amber force field. *J. Comput. Chem.* **2004**, *25*, 1157−1174.
(34) Darden, T.; York, D.; Pedersen, L. Particle Mesh Ewald—an N.Log (N) method for Ewald sums in large systems. *J. Chem. Phys.* **1993**, *98*, 10089−10092.
(35) Ryckaert, J. P.; Ciccotti, G.; Berendsen, H. J. C. Numerical integration of the Cartesian equations of motion of a system with constraints: molecular dynamics of *n*-alkanes. *J. Comput. Phys.* **1977**, *23*, 327−341.
(36) Kollman, P. A.; Massova, I.; Reyes, C.; Kuhn, B.; Huo, S.; Chong, L.; Lee, M.; Lee, T.; Duan, Y.; Wang, W.; Donini, O.; Cieplak, P.; Srinivasan, J.; Case, D. A.; Cheatham, T. E. Calculating structures and free energies of complex molecules: combining molecular mechanics and continuum models. *Acc. Chem. Res.* **2000**, *33*, 889−897.
(37) Anand, O.; Yu, L. X.; Conner, D. P.; Davit, B. M. Dissolution testing for generic drugs: an FDA perspective. *AAPS* **2013**, *13*, 328−335.
(38) Mosmann, T. Rapid colorimetric assay for cellular growth and survival: application to proliferation and cytotoxicity assays. *J. Immunol. Methods* **1983**, *65*, 55−63.
(39) Pascall, B.; Maud, G.; Georges, D.; Adelin, A.; Valery, B.; Bruno, P.; Didier, C.; Geraldine, P.; Luc, D.; Brigitte, E. The effect of cyclodextrins on aqueous solubility of a new MMP inhibitor: phase solubility, $^{1}$H NMR spectroscopy, molecular modeling studies, preparation and stability study of nebulizable solutions. *J. Pharm. Sci.* **2005**, *8*, 164−175.
(40) Forgo, P.; Gondos, G. A study of $\beta$-cyclodextrin inclusion complexes with progesterone and hydrocortisone using rotating frame overhauser spectroscopy. *Monatsh. Chem.* **2002**, *133*, 101−106.
(41) Madan, J.; Dhiman, N.; Sardana, S.; Aneja, R.; Chandra, R.; Katyal, A. Long circulating poly (ethylene glycol)-grafted gelatin nanoparticles customized for intracellular delivery of noscapine: preparation, in-vitro characterization, structure elucidation, pharmacokinetic and cytotoxicity analysis. *Anticancer Drugs* **2011**, *22*, 543−555.
(42) Olsson, B.; Bolme, P.; Dahlstrom, B.; Marcus, C. Excretion of noscapine in human breast milk. *Eur. J. Clin. Pharmacol.* **1986**, *30*, 213−215.
(43) Fan, L. F.; He, W.; Chang, Y. Z.; Xiang, B.; Du, Q.; Wang, F.; Qin, M.; Cao, D. Y. Studies on chitosan/Kollicoat SR30D film coated tablets for colonic drug delivery. *Int. J. Pharm.* **2009**, *375*, 8−15.
(44) Ungell, A. L.; Nylander, S.; Bergstrand, S.; Sjoberg, A.; Lennernas, H. Membrane transport of drugs in different regions of the intestinal tract of the rat. *J. Pharm. Sci.* **1998**, *87*, 360−366.